

MECHANISMS INVOLVED IN SPIKE FREQUENCY ADAPTATION OF A TYPE S MOTONEURON: A COMPUTATIONAL STUDY

E. J. Fernandes*, Renata C. Barbosa* and M. F. Vieira*

*Bioengineering and Biomechanics Laboratory, UFG, Goiânia, Brazil

e-mail: marcus.fraga.vieira@gmail.com

Abstract: A computational model was developed to evaluate the influence of the calcium-dependent potassium conductance (g_{KCa}), the calcium concentration in soma (varying the velocity of calcium extrusion - vel_{ext} - and the calcium conductances in soma - g_{CaN} and g_{CaP}), the inclusion of a slow inactivation state variable in soma's fast sodium conductance and the conductance of the persistent sodium current in the initial segment (g_{NapSI}) in the spike-frequency adaptation of a type S motoneuron. Blocking g_{KCa} in the model eliminated the initial phase of the spike frequency adaptation and so, this phase was associated with the AHP. Early adaptation was abolished when, in the reference model, the g_{NapSI} was blocked. The inclusion of a slow inactivation variable in the fast sodium conductance enables a late adaptation phase and also affects the early phase so, these phases are related with currents of large time constants (about 20s).

Keywords: adaptation, motoneuron, mathematical modeling.

Introduction

The spike frequency adaptation is a property that occurs in response to a sustained input. In the passive condition, motoneurons (MN) show a decrease in the firing rate that is time-dependent. Adaptation is divided into three phases:

- a) initial phase: limited to the first few action potentials (AP) with a linear characteristic [1];
- b) early phase: the first few hundred milliseconds of firing with an exponential characteristic and time constant of about 250 ms [1];
- c) late phase: can last for tens of seconds or even minutes, also with an exponential characteristic and time constant of 10 to 20s [2, 3].

The mechanisms involved in spike frequency adaptation are not well understood. Considerable attention has been given to the role of afterhyperpolarization (AHP), which is mediated by calcium-dependent potassium (SK-type) conductance. The increase in intracellular calcium concentration during repetitive firing increases the activation of calcium dependent potassium channels, which, in turn, causes the summation of AHP [4] leading to a progressive increase in the intervals between AP and, therefore, a reduction in firing frequency. In addition, some experimental and theoretical studies have demonstrated the existence of spike frequency adaptation

independent of the AHP [1, 5, 6]. In this situation, the conductances responsible for the action potential appear to be involved in the adaptation, especially the slow inactivation of fast sodium conductance [5] and the persistent sodium currents [7].

Thus, given the inconclusive results obtained so far, the aim of this study was to investigate the mechanisms involved in the spike frequency adaptation in MNs through computer simulations, in order to investigate the role of different mechanisms in the different phases of spike frequency adaptation in MNs.

Material and methods

Model architecture – The type S MN model (S – slow) was developed from the work of Vieira and Kohn [8], but with a different geometry. It presents a cylindrical initial segment, a spherical soma, a dendritic tree modeled with one stem dendrite and two asymmetrical dendritic branches using a tapering cable model: the largest dendritic branch has ten cylindrical compartments and the smallest one has eight compartments. The model was adjusted to fit data from cat MN [9].

Nine different conductances were modeled in the soma (coupling, leak, fast sodium, delayed rectifier potassium, SK-type potassium, BK-type potassium, hyperpolarizing, A conductance, N- and P-type calcium), five in the initial segment (leak, coupling, fast sodium, delayed rectifier potassium and persistent sodium) and two in each dendritic compartment (leak and coupling).

The model equations were written according to the Hodgkin and Huxley's formalism [10].

The slow inactivation of sodium channels was modeled by including a state variable with an infinite curve of low slope and high time constant in the fast sodium conductance equations, as suggested by Miles and colleagues [6].

The model was written in C++ language to run in a Windows environment, ensuring portability and fast processing. The differential equations were integrated using the 4th order Runge-Kutta algorithm with fixed time steps of 0.01 ms. Scripts were written in Matlab to evaluate the results and generate the simulations graphs.

Tests protocols – A current pulse of 50 nA and 0.5 ms of duration was injected into the soma to generate an action potential and verify the AHP characteristics, comparing them with data from cat MNs [9]. To evaluate

the adaptation in the model, a step current of 30 nA and 6.0 s of duration was injected in the soma.

The influence of each possible mechanism involved in spike frequency adaptation was tested by varying the calcium-dependent potassium conductance (g_{KCa}); by changing the calcium concentration in the soma (varying the calcium velocity of extrusion from the cell - vel_{ext} - and varying the calcium conductances in soma - g_{CaN} and g_{CaP}); by including a slow inactivation state variable in the equations of fast sodium conductances of the soma and of the initial segment (g_{Nas}) and varying the persistent sodium conductance in the initial segment (g_{NapSI}). Values of 0%, 80%, 100% and 120% of the reference value were tested. The 0% value represents the blockade of the corresponding variable in the model (assigning zero to its conductance value). We analyzed the adaptation by blocking simultaneously g_{KCa} and g_{NapSI} and evaluated the model behavior by blocking g_{NapSI} and keeping g_{Nas} in the model.

Results

The model used as reference for the other tests was adjusted with the following AHP characteristics: -5.032 mV of amplitude, half-decay of 50.99 ms and 152.31 ms of duration, values that are within the experimentally reported range [9].

Blocking g_{KCa} conductance generated the largest maximum instantaneous firing frequency ($freq_{max}$) and steady state frequency ($freq_{ss}$) observed in all conditions tested in the model. Figure 1 shows the typical instantaneous frequency *versus* duration of the stimulus curve for the different values of g_{KCa} tested.

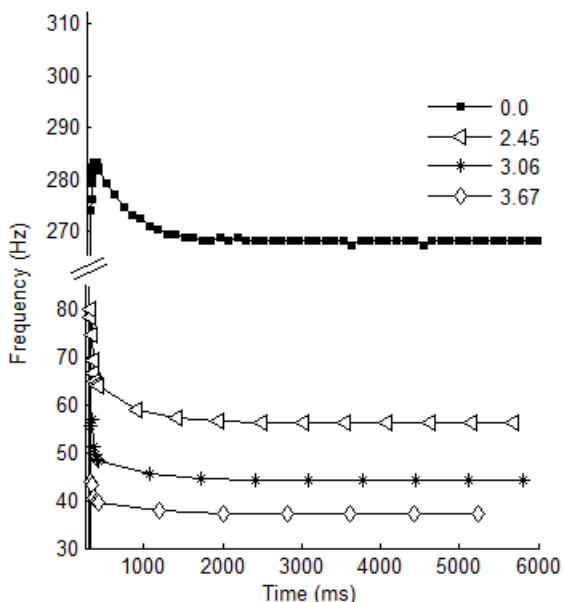


Figure 1: Spike frequency adaptation for different values of g_{KCa} (in mS).

When g_{KCa} was completely blocked ($g_{KCa} = 0.0$ mS), the AHP was abolished, but it remained within the

experimental values for all the other values of g_{KCa} tested. As these conductance increased, the AHP amplitude increased and the firing rate decreased.

The reference value for calcium extrusion velocity was 3.4 $\mu\text{m}/\text{ms}$. When using 80% and 120% of this value, the AHP amplitude remained within the experimental values, but the values for half-decay and duration of AHP became very large (to 80%) or very small (to 120%), very different from what is experimentally measured [9].

The influence of calcium concentration in the soma was also evaluated by changing the values of g_{CaN} and g_{CaP} . Blocking g_{CaN} generated $freq_{max}$ equal to 137.6 Hz and $freq_{ss}$ equal to 65.49 Hz, and blocking g_{CaP} generated $freq_{max}$ equal to 184.5 Hz and $freq_{ss}$ equal to 80.97 Hz. As the values of these conductances increased, the corresponding $freq_{max}$ and $freq_{ss}$ values decreased, and the AHP magnitude, half-decay and duration increased.

Blocking g_{NapSI} generated an AHP with large amplitude (-6.443 mV) and the other tested values for this conductance produced an AHP with smaller amplitudes. Figure 2 shows the influence of this conductance on adaptation. It was observed that g_{NapSI} causes an acceleration in the MN firing frequency, but it also increases the time constant of the early adaptation.

Simultaneously blocking g_{KCa} and g_{NapSI} abolished the spike frequency adaptation.

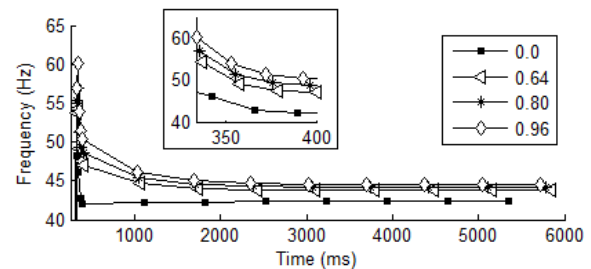


Figure 2: Influence of g_{NapSI} on firing frequency adaptation (values in mS). Inset: zoom showing the initial adaptation.

The inclusion of a slow inactivation state variable in the fast sodium conductance of soma and initial segment caused the spike frequency adaptation shown in Figure 3 - g_{Nas} . When we included this state variable and blocked g_{NapSI} , we generated the spike frequency adaptation curve shown in Figure 3 - g_{Nas} without g_{NapSI} .

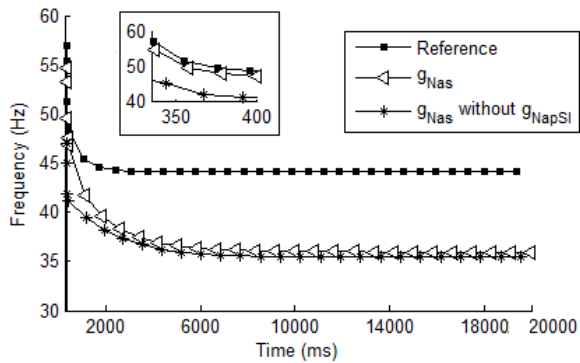


Figure 3: Model response to a sustained current input of 30 nA and 20s of duration for the reference model, the model including a slow inactivation state variable in fast sodium (g_{NaS}) and the with g_{NaS} and g_{NaPSI} blocked. Inset: zoom showing the initial adaptation.

Discussion

Blocking g_{KCa} in the model led to high firing rates for sustained current input. This blockade mimics the effect of apamin in the MN, which blocks the calcium-dependent potassium currents [5]. Considering this conductance represents the potassium channels responsible for the AHP and that the AHP is a limiting factor for the firing rate [5], it was expected that its blockade would cause an increase in the firing rate, as observed in these simulations. Figure 1 (case $g_{KCa} = 0.0$ mS) shows that the initial phase is abolished when this conductance is blocked (there is no linear characteristic during the first few spikes). Studies indicated that the initial adaptation happens because the calcium concentration increases progressively during successive spikes, and, once the potassium conductance that underlies AHP depends on intracellular calcium concentration, the AHP of the second spike will be more longer than that of the first spike, creating a limiting factor that causes a decrease in the firing rate for the first few spikes after the input of a sustained current [11, 12].

Blocking g_{KCa} could not abolish the early phase of spike frequency adaptation and neither the late phase (Figure 1, case 0.0 mS), similar to what is reported by some other studies [5, 6]. In our model, however, the spike frequency adaptation was less abrupt than that reported by these studies (the difference between $freq_{max}$ and $freq_{ss}$ was lower in our study) and, also, it is possible to see that there is an acceleration during the first milliseconds after current injection that was not reported in these other studies [5,6]. In a modeling study, blocking a conductance completely eliminates its corresponding current whereas in experimental studies, a perfect blockade is hard to be reached. The results from the studies mentioned above for g_{KCa} blockade resemble our study when, in the model, g_{KCa} is decreased, but not completely abolished.

Changes in the velocity of extrusion affected mainly the duration and half-decay of AHP, limiting the firing rate. The higher the extrusion velocity, the lower will be

the AHP and, consequently, the higher will be the firing rate of the MN.

Blocking, increasing or decreasing the calcium conductances (g_{CaN} e g_{CaP}) led to similar results for AHP characteristics and spike frequency adaptation. These changes affected calcium-dependent potassium currents and, therefore, indirectly affected AHP [11]. The higher these conductances, the higher the calcium influx to the cell and, therefore, more calcium-dependent potassium conductance could be active due to this influx causing a higher AHP amplitude and duration and, consequently lower firing rates could be reached.

Blocking the persistent sodium current – setting its conductance to zero – blocked the early adaptation. Figure 2 shows how, for the case in which g_{NaPSI} was blocked, the typical exponential decay of this phase ceased. Slow inactivation processes can be related to the progressive increase of firing threshold, causing the early and late phases of spike frequency adaptation, once they have large time constants [12]. Zeng and colleagues, however, could not block the late adaptation when they used a blocker for the persistent sodium currents in an experiment with rat hypoglossal MNs and concluded that several channels may affect spike frequency adaptation [7]. In our model, the time course of the initial segment's persistent sodium current are related with the time course of the early adaptation, perhaps because this current was the only one included in our model that was modeled with a persistent mechanism.

When we blocked, in the reference model, the persistent sodium conductance of the initial segment and the calcium-dependent potassium current conductance in soma, we could cease all phases of adaptation. Thus, both of these conductances appear to be directly related with the MN's spike frequency adaptation.

The inclusion of a slow inactivating mechanism in the fast sodium conductance added another slow inactivating mechanism to the model, and, then, the model could reproduce a spike frequency adaptation more similar to that experimentally reported [5, 6], reproducing, in addition to the early phase, the late one (see Figure 3 - g_{NaS}). In our study, blocking g_{NaPSI} ceased early adaptation (Figure 2, $g_{NaPSI} = 0.0$ mS) that was not identified by Miles and colleagues [6], perhaps, because we did not include in the reference model the slow inactivation variable for the fast sodium conductance. In addition to Miles and colleagues [6] results, g_{NaPSI} seems to influence the early phase of spike frequency adaptation and, blocking it, decreases the firing frequency during this phase (see Figure 3, g_{NaS} without g_{NaPSI}).

Conclusion

Tests performed in our model indicated that the conductance responsible for AHP (g_{KCa}) influences the initial phase of spike frequency adaptation, whereas the early and late phases are related to the persistent sodium conductance and the slow inactivation of fast sodium conductance. So each adaptation phase appears to be controlled by separated mechanisms. Once the MN also

has several other channels that activate and inactivate during repetitive firing, differences between spike frequency adaptation in our model and the experimental tests might be related to mechanisms that were not included in model for simplification purposes, as a more detailed dendritic tree and/or the inclusion of dendritic persistent inward currents (despite this latter current is not present in slice preparations). Further studies, in which the model mimics the responses obtained through experimental studies and includes more identified motoneurons features, may provide new clues to elucidate the mechanisms underlying the spike frequency adaptation.

Acknowledgments

The first and the second author acknowledge CAPES for Master's scholarship. The first author acknowledges FAPEG for financial support.

References

- [1] Sawczuk A, Powers RK, Binder MD. Spike frequency adaptation studied in hypoglossal motoneurons of the rat. *Journal of Neurophysiology*. 1995; 73:1799-810.
- [2] Kernell D. The adaptation relation between discharge frequency and current strength of cat lumbosacral motoneurons stimulated by long-lasting injected currents. *Acta Physiologica Scandinavica*. 1965; 65:65-73.
- [3] Kernell D, Monster AW. Time course and properties of late adaptation spinal motoneurons of the cat. *Experimental Brain Research*. 1982; 46:191-96.
- [4] Granit R, Kernell D, Shortess GK. Quantitative aspects of repetitive firing in mammalian motoneurons caused by injected currents. *Journal of Physiology*. 1963; 168:911-31.
- [5] Viana F, Bayliss DA, Berger AJ. Multiple potassium conductances and their role in action potential repolarization and repetitive firing behavior of neonatal rat hypoglossal motoneurons. *Journal of Neurophysiology*. 1993; 69:2150-63.
- [6] Miles A, Dai Y, Brownstone RM. Mechanisms underlying the early phase of spike frequency adaptation in mouse spinal motoneurons. *Journal of Physiology*. 2005; 566(2):519-32.
- [7] Zeng J, Powers RK, Newkirk G, Yonkers M, Binder MD. Contribution of persistent sodium currents to spike-frequency adaptation in rat hypoglossal motoneurons. *Journal of Neurophysiology*. 2005; 93:1035-41.
- [8] Vieira MF, Kohn AF. Compartmental models of mammalian motoneurons and their computer simulation. *Computers in Biology and Medicine*. 1995; 37:842-60.
- [9] Zengel JE, Reid SA, Sybert GW, Munson JB. Membrane electrical properties and prediction of motor unit type of medial gastrocnemius of motoneurons in the cat. *Journal of Neurophysiology*. 1985; 53(5):1323-44.
- [10] Hodgkin AL, Huxley AF. A quantitative description of membrane current and its application to conduction and excitation in nerve. *Journal of Physiology*. 1952; 117(4):500-54.
- [11] Kernell D. Motoneurons: electrophysiology. Em: D. Kernell, editor. *The Motoneurons and its Muscle Fibres*. New York: Oxford; 2006. p. 97-133.
- [12] Sawczuk GB, Powers RK, Binder MD. Contribution to spike-frequency adaptation in hypoglossal motoneurons of the rat. *Journal of Neurophysiology*. 1997; 78:2246-53.